MIT JOINT PROGRAM
SCIENCE POLICY
GLOBAL CHANGE

Report 358
March 2022

Assessing the Changing Risk of Flood-producing Events in Cambridge

Xiang Gao and C. Adam Schlosser

MIT Joint Program on the Science and Policy of Global Change combines cutting-edge scientific research with independent policy analysis to provide a solid foundation for the public and private decisions needed to mitigate and adapt to unavoidable global environmental changes. Being data-driven, the Joint Program uses extensive Earth system and economic data and models to produce quantitative analysis and predictions of the risks of climate change and the challenges of limiting human influence on the environment—essential knowledge for the international dialogue toward a global response to climate change.

To this end, the Joint Program brings together an interdisciplinary group from two established MIT research centers: the **Center for Global Change Science (CGCS)** and the **Center for Energy and Environmental Policy Research (CEEPR)**. These two centers—along with collaborators from the Marine Biology Laboratory (MBL) at Woods Hole and short- and long-term visitors—provide the united vision needed to solve global challenges.

At the heart of much of the program's work lies MIT's Integrated Global System Model. Through this integrated model, the program seeks to discover new interactions among natural and human climate system components; objectively assess uncertainty in economic and climate projections; critically and quantitatively analyze environmental management and policy proposals; understand complex connections among the many forces that will shape our future; and improve methods to model, monitor and verify greenhouse gas emissions and climatic impacts.

This report is intended to communicate research results and improve public understanding of global environment and energy challenges, thereby contributing to informed debate about climate change and the economic and social implications of policy alternatives.

—Ronald G. Prinn,
Joint Program Director

MIT Joint Program on the Science and Policy of Global Change

Massachusetts Institute of Technology
77 Massachusetts Ave., E19-411
Cambridge MA 02139-4307 (USA)

T (617) 253-7492 **F** (617) 253-9845
globalchange@mit.edu
http://globalchange.mit.edu/

GLOBAL CHANGE

MARCH 2022

Assessing the Changing Risk of Flood-producing Events in Cambridge

Xiang Gao[1] and C. Adam Schlosser

Abstract: In this study, we assess the potential for future changes in the frequency of summertime heavy-to-extreme precipitation events – defined as 2" of rainfall in 3 hours – across the greater Cambridge area as a result of anthropogenic global warming. The study relies upon an "analogue method" that identifies well-resolved large scale, daily-averaged atmospheric patterns associated with the occurrence of local extreme events, and thus enables evaluating the ability of climate models to simulate conditions conducive to such extremes that occur at unresolvable spatial scales. We find that climate models from the Phase 5 of the Coupled Model Intercomparison Project (CMIP5) consistently reproduce the historical occurrence of these synoptic-scale patterns associated with the occurrence of the heavy-to-extreme precipitation events observed across the greater Cambridge area. Applying these analogues into the future across all the CMIP5 model projections, there is weak evidence of any considerable trend in the frequency of these heavy-to-extreme events out to the end of the 21st century. Furthermore, analyses that consider a strong climate-change mitigation scenario show no salient effect on the ensemble-median change as well as the interquartile and minimum-maximum ranges. Further work is warranted that considers: a more robust sampling of associated spatial patterns, rather than a pooled or average spatial pattern, to the local extreme; a more explicit treatment of the sub-daily atmospheric patterns that coincide with the local, sub-daily (i.e., 3-hour) event.

1. INTRODUCTION **2**
2. METHOD AND DATASETS **2**
2.1 METHOD 2
2.2 DATASETS 2
2.3 DATA PROCESSING 3
3. RESULTS **4**
3.1 SYNOPTIC CONDITION COMPOSITES 4
3.2 CALIBRATION OF ANALOGUE DETECTION DIAGNOSTICS 4
3.3 HISTORICAL FLOOD PRODUCING EVENT FREQUENCY 5
3.4 PROJECTED FUTURE CHANGES IN FLOOD PRODUCING EVENT FREQUENCY 6
4. SUMMARY REMARKS **7**
5. REFERENCES **7**

1 Corresponding author (Email: xgao304@mit.edu)
Joint Program on the Science and Policy of Global Change, Massachusetts Institute of Technology, MA, USA

1. Introduction

MIT Flood Vulnerability Study is one key part of a broader initiative led by the MIT Climate Resiliency Committee (CRC) and the MIT Office of Sustainability (MITOS) to understand and recommend how MIT can continue to fulfill its mission in the face of intensifying climate risks over the next 100 years and beyond. The risks include heavy precipitation induced flooding, sea level rise/storm surge, and chronic heat stress. The overall objective is to translate the scientific understanding of current and future campus-based flooding risks from climate change into operational and strategic guidance for informing campus planning and management.

Since 2010, there have been several severe thunderstorms dumping drenching rain across different parts of Boston area (**Table 1**). In this study, we present an application of our recently developed "analogue method" to assess the changing risk of flood-producing summer rainstorm over Cambridge, Massachusetts under future climate. The analogue method has been demonstrated to successfully detect the occurrence of heavy precipitation and heat wave events across different regions of United States with satisfactory performances (Gao *et al.*, 2014; Gao *et al.*, 2017; Gao *et al.*, 2018; Gao and Schlosser, 2019). This is our initial effort to apply the method for detecting pluvial flood producing events at the city scale.

2. Method and datasets

2.1 Method

The analogue method has been described in detail in Gao *et al.* (2014, 2017), so we briefly elaborate it here. The method employs "composites" to identify prevailing large-scale atmospheric conditions (i.e., circulation features, moisture plumes) associated with the observed heavy precipitation events at local scale, through the joint analyses of precipitation-gauge observations and atmospheric reanalysis. The model-simulated daily meteorological conditions are then evaluated against the composites for their similarities in terms of the established "criteria of detection" (described later). Any day when the criteria of detection are met would be considered as a heavy precipitation day. Therefore, the analogue method only allows for the characterization of the heavy precipitation frequency.

2.2 Datasets

U.S. hourly precipitation observations, archived at the National Climatic Data Center (NCDC) (https://data.nodc.noaa.gov/cgi-bin/iso?id=gov.noaa.ncdc:C00313), is based on the collection of approximately 7,000 US National Weather Service (NWS), Federal Aviation Administration (FAA), and cooperative observer stations in the United States of America, Puerto Rico, the US Virgin Islands, and various Pacific Islands. The measurement represents hourly precipitation accumulation. The temporal coverage of the data varies considerably by state and region. At most of stations in Cambridge/Boston area (**Figure 1** and **Table 2**), the hourly precipitation is available from 1979-2013.

The Modern-Era Retrospective analysis for Research and Applications, Version 2 (MERRA-2) provides data beginning in 1980 at a spatial resolution of 0.625° × 0.5° (Bosilovich *et al.*, 2016). In comparison with the original MERRA dataset, MERRA-2 represents the advances made in both the Goddard Earth Observing System Model, Version 5 (GEOS- 5) (Molod *et al.*, 2015) and the Global Statistical Interpolation (GSI) assimilation system that enable assimilation of modern hyperspectral radiance and microwave observations, along with GPS-Radio Occultation datasets. MERRA-2 is the first long-term global reanalysis to assimilate space- based observations of aerosols and represent their interactions with other physical processes in the climate system. In this study, we use the three-dimensional daily atmospheric diagnostics on 42 pressure levels. The MERRA-2 reanalysis is mainly employed to construct the large-scale composites of atmospheric patterns associated with identified observed rare precipitation events and calibrate the analogue scheme.

We also compile the climate model simulations from the CMIP5 historical experiment (years 1850–2005) and experiment for the twenty-first century (years 2006–2100) employing the RCP 4.5 and 8.5 scenarios. The historical runs were forced with observed time-evolving land cover and temporal variations of anthropogenic and natural forcings. The two future scenarios represent social and economic development consistent with radiative forcing paths of 4.5 W/m^2 and 8.5 W/m^2 by year 2100, respectively. 18 models provide all the essential daily meteorological variables for the analogue schemes across the experiments (Gao *et al.*, 2017), 4 of which provide data from several initial condition

Table 1. Severe thunderstorms occurring on parts of Boston area since 2010

Location	Date	Rain (inches)	Time Span (hour)
Cambridge	July 10, 2010	3.5	1
Logan Airport	March 20, 2014	3	24
Maynard/Dorchester	August 2, 2017	4	2
Lynn	September 30, 2017	4	1
Lynn	August 12, 2018	8	2

ensemble members. In this study, we consider only one ensemble member of each CMIP5 model.

2.3 Data processing

In this study we focus on a pluvial flood producing summer (June-July-August, JJA) rainstorm, defined as "excessive rainfall rate larger than or equal to 2" across a 3-hour period. The hourly precipitation observations from all the stations surrounding the city of Cambridge (e.g., Figure 1 and Table 2) are extracted to identify such events. At each station, we first generate a continuous 3-hour running total across the entire period when the observations are available and then identify any date when precipitation amount in any 3-hour window exceeds 2". For any event across the consecutive

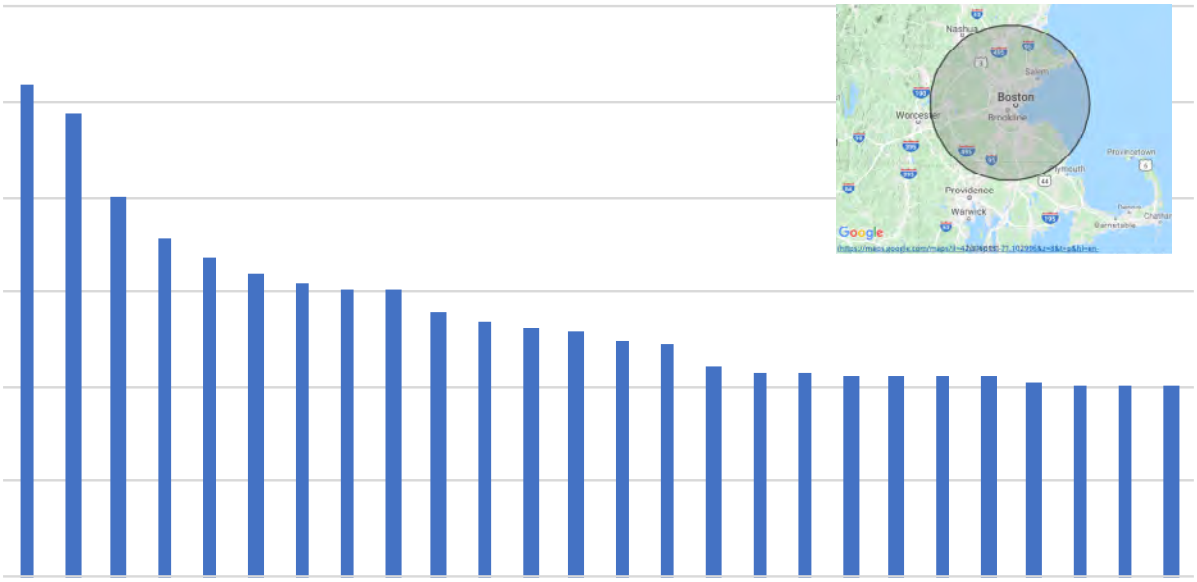

Figure 1. Barplot shows the 3-hour storm totals that were extracted from hourly gauged-based precipitation observations (1979-2013) taken at stations surrounding Cambridge, MA. The shaded region in the inset map depicts the radius of the surrounding area from which the station observations were pooled.

Table 2. Summary of the 3-hour storm totals that were extracted from hourly gauged-based precipitation observations (1979-2013) taken at stations surrounding Cambridge, MA. For each entry, the station, date (YYYYMMDD) and time (local), and 3-hour total (inches) is provided.

Station	Date	3-hour Storm total (Inches)
MARBLEHEAD MA	19930325 16:00	5.19
BELLINGHAM MA	19860607 18:00	4.88
BRIDGEWATER MA	19900724 13:00	4
BOSTON MA	19850801 03:00	3.58
BLUE HILL MA	19980613 16:00	3.38
BLUE HILL MA	19980613 15:00	3.2
BLUE HILL MA	19980618 16:00	3.08
BOSTON MA	19850801 02:00	3.03
BOSTON MA	19980613 16:00	3.02
BRIDGEWATER MA	19900724 12:00	2.8
BLUE HILL MA	20050814 16:00	2.68
BLUE HILL MA	19880727 08:00	2.62
MARBLEHEAD MA	19880401 00:00	2.59

Station	Date	3-hour Storm total (Inches)
BELLINGHAM MA	19900811 10:00	2.5
BLUE HILL MA	19980613 14:00	2.46
MARBLEHEAD MA	19850801 04:00	2.2
BOSTON MA	20100825 10:00	2.16
BOSTON MA	20070728 17:00	2.16
BELLINGHAM MA	19950725 15:00	2.1
BRIDGEWATER MA	19900724 10:00	2.1
BRIDGEWATER MA	19860807 19:00	2.1
MARBLEHEAD MA	19980613 18:00	2.1
BLUE HILL MA	19880727 05:00	2.06
BELLINGHAM MA	19800729 17:00	2.02
BLUE HILL MA	19860807 17:00	2.02
BRIDGEWATER MA	19900620 06:00	2

days, we only account the event once, specifically on the first day. Non-overlapping dates from all the stations are pooled together as the total observed events.

The same set of meteorological variables are assembled or derived from the MERRA-2 reanalysis and CMIP5 climate model simulations, including 500 hPa vector winds (uv_{500}), 500 hPa vertical velocity (w_{500}), near-surface specific humidity (q_{2m}), and total column precipitable water (tpw). These fields represent key environmental conditions during extreme precipitation development and are readily available in the output archives of most of the models involved in the various model intercomparison projects. Our analogue schemes are constructed based on a combination of 500 hPa horizontal and vertical winds (uvw_{500}) and choice of two moisture variables (near-surface specific humidity and total column precipitable water), hereinafter referred to as $uvw_{500}q_{2m}$ and $uvw_{500}tpw$, respectively. All the daily meteorological fields from MERRA-2 reanalysis and CMIP5 climate models are regridded to the common 2.5°x2° resolution through conservative regridding as suggested by Chen and Knutson (2008).

At each grid cell, we convert the meteorological fields to standardized anomalies based on the seasonal climatological mean and standard deviation of 1980-2013 for MERRA-2 reanalysis but those of 1980-2005 for the CMIP5 historical experiment. The additional several years for MERRA-2 are included to ensure that sufficient number of observed events are available to calibrate the analogue scheme. The same 26-year (1980-2005) seasonal climatological means and standard deviations are also employed to calculate the standardized anomalies for the meteorological fields of CMIP5 RCP experiments from 2006 to 2100. The projected changes in event frequency for CMIP5 experiments focus on seven 26-year periods centered at the years 2020, 2030, 2040, 2050, 2060, 2070, and 2080, respectively. So the first period spans from 2008 to 2033, and so on. The change in event frequency of each model is assessed relative to its respective seasonal value from 1980 to 2005 and expressed as number of events per year.

3. Results

3.1 Synoptic condition composites

We extract 95 events from the observations of 1980-2013 for the summer season (JJA) of Cambridge. **Figure 2** shows the composites as standardized anomalies, produced by averaging the MERRA Reanalysis across the observed event days. The presented various atmospheric fields provide an insight into the preferred synoptic conditions conducive to these events. We see very strong southerly winds transport warm and moist air from the ocean. The study region is also characterized by a very strong upward motion that carries a lot of moisture (Fig. 2b). The presence of flanking circulations (lower heights to the west and higher heights to the east of New England) energize these two conditions.

3.2 Calibration of analogue detection diagnostics

We follow the same procedure as described in Gao *et al.* (2017) to develop and calibrate the analogue scheme and will briefly state it here. Two metrics, the "hotspot" and the spatial anomaly correlation coefficient (SACC) are employed to characterize the degree of consistency between daily MERRA-2 atmospheric fields and the distinct synoptic conditions conducive to flood-producing events shown in composites. The "hotspot" metric diagnoses the extent to which the composite of each atmospheric field is representative of any individual event. It involves the calculation of sign count at each grid cell by recording the number of individual events whose standardized anomalies have consistent sign with the composite. "Hotspots" are identified as the grid cells where the events used to construct the composites exhibit strong

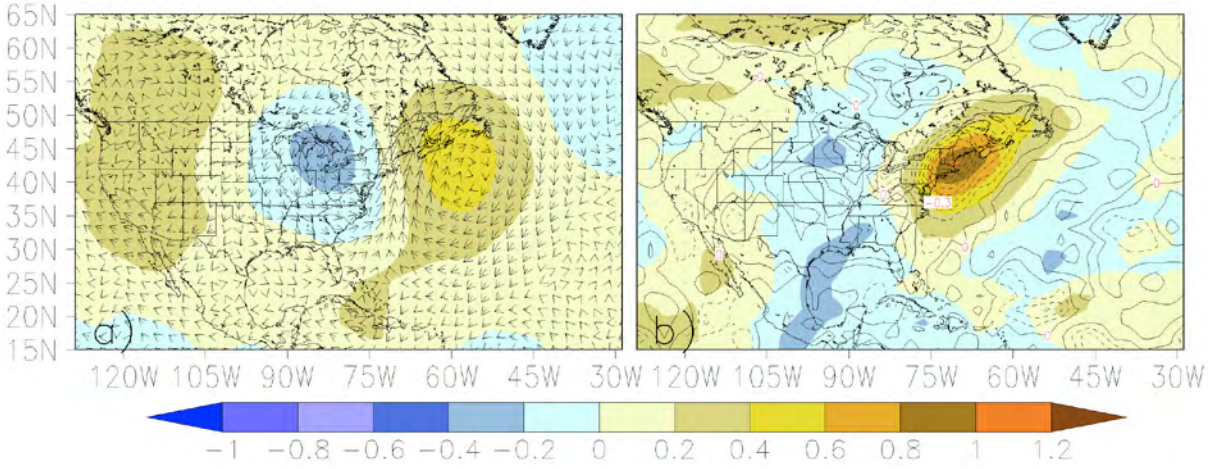

Figure 2. Composite fields as normalized anomalies for DJF in Boston. (a) 500-hPa geopotential height (shaded, h500) and the vertical integrated water vapor flux vector up to 500 hPa (arrow) based on 95 flood producing events at 2.5°x2°. (b) 500-hPa vertical velocity (contour, ω500) and total precipitable water (*tpw*, shaded).

sign consistency with the composite itself (i.e., the larger sign counts). SACC is calculated between the daily MERRA-2 atmospheric fields and the corresponding composites over the region that captures and centers the coherent structures of the composite fields. Previous analyses from Gao *et al.* (2017) found that the resulting optimal thresholds (described later) is not sensitive to the differences in the size and aspect ratio of regions chosen for SACC calculation. Ten ranges of SACC threshold are assessed from 0.0 to 1.0 with an interval of 0.1. We perform automatic calibration to determine the cut-off values for SACC and the number of hotspots of all four variables simultaneously. Five performance measures are adopted that are commonly used in "confusion matrix" for binary classification, including True Positive Rate (TPR), False Positive Rate (FPR), Accuracy (ACC, the ratio of combined true positives and true negatives to total population), Precision (PPV, the proportion of correctly identified events to the total identified heavy events), and F1 score (the harmonic mean of PPV and TPR). We examined two criteria for detection of flood-producing events in this study: (1) at least 3 out of 4 variables have consistent signs with the corresponding composites over the selected "hotspot" grid cells; and (2) at least 3 out of 4 variables have SACCs larger than the determined thresholds (referred to as "Criteria1" or "C1") or at least 2 out of 4 variables have SACCs larger than the determined thresholds but the SACCs of all four variables have to be positive (referred to as "Criteria2" or "C2"). The optimal cutoff values for the number of hotspots and SACC threshold are chosen to produce the observed number of events with the best TPR. The established detection criteria will then be applied to the CMIP5 historical and future model-simulated daily meteorological conditions to obtain analogue-based events. Note that when considering future climate, we assume stationarity of the synoptic-scale states and that climate change will, for the most part, manifest itself as a change in the timing, persistence, and frequency of these large-scale features. We compare the results of analogue scheme in the historical period with the events identified from the observations.

The calibration of analogue scheme based on the combination of two criteria (C1 vs. C2) and two moisture variables (*tpw* vs. q_{2m})) leads to the TPR of 27.4 ~ 28.4% and FPR of 2.2 ~ 2.3% under the constraint of producing the observed number of events from 1980 to 2013. The TPR improves to 34.7 ~ 41.1% and 37.9 ~ 44.2% if the window for matching dates is enlarged to ±1 and ±2 days, respectively. We found no single scheme to perform the best consistently.

3.3 Historical flood producing event frequency

We then apply various analogue schemes to the CMIP5 late twentieth-century model simulations and examine the capabilities of current state-of-the-art climate models to realistically replicate the "resolved" large-scale atmospheric conditions associated with flood-producing events. Validating the circulation behaviors linked to these events in climate models can ensure the assessment of their future changes with greater confidence. This is achieved by judging the CMIP5 model-simulated daily meteorological conditions of 1980 to 2005 against the constructed composites (in Fig. 2) for their similarity based on the established criteria of detection. In this way, any day when the criteria of detection are met would be considered as a flood-producing event. We then compare the results of the analogue schemes with the events identified from the observations (**Figure 3**).

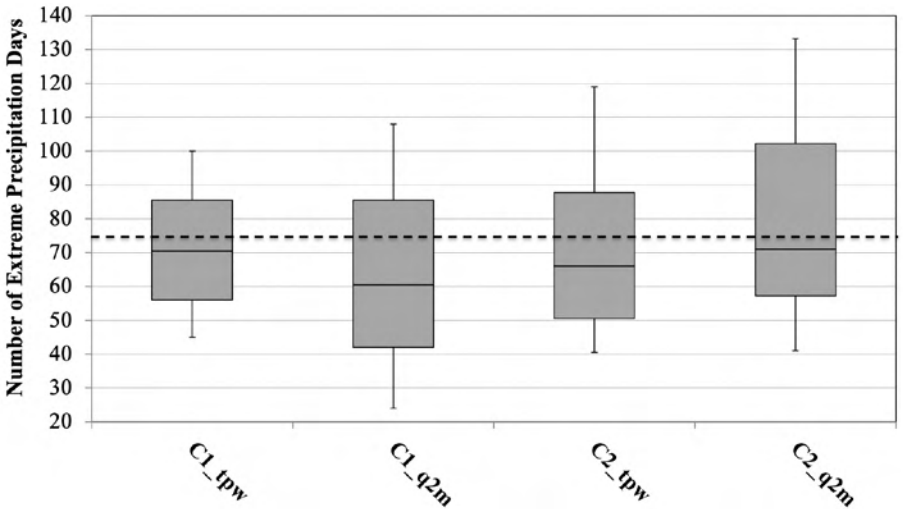

Figure 3. Comparisons of the number of summer season (JJA) flood-producing events in Cambridge estimated from the CMIP5 model-simulated atmospheric synoptic conditions based on various analogue schemes during the period of 1980 to 2005. The whisker plot shows the minimum, the lower and upper quartile, median, and the maximum across 18 CMIP5 models. The dashed lines indicate the number of flood-producing events identified from the gridded observations at 2.5x 2º.

Multi-model medians of all the analogue schemes indicate the underestimate of flood-producing event frequency in comparison with the observation. Depending on the choice of the scheme, the underestimation ranges from 3.0 ~ 13.5 days but interquartile range and inter-model spread can vary widely. The scheme "C1_tqv" performs the best among all with its multi-model median the most consistent with the observation and the smallest inter-quartile range and inter-model spread. Nevertheless, no single criteria or moisture variable performs consistently better than the other one.

3.4 Projected future changes in flood producing event frequency

We convert the CMIP5 model-simulated daily meteorological fields from 2006 to 2100 to standardized anomalies relative to the seasonal climatological means and standard deviations of each model from the CMIP5 historical simulations (1980–2005). We analyze the projected changes in flood producing event frequency during seven 26-yr periods centered at the years 2020, 2030, 2040, 2050, 2060, 2070, and 2080, respectively. So the first period spans from 2008 to 2033, and so on. The change of each model is calculated relative to its respective seasonal event frequency from 1980 to 2005 and expressed as number of events per year. This is done for all the four analogue schemes.

We find that the multi-model median from none of analogue schemes produces a frequency change that is greater than 1 event per season across all the seven epochs (**Figure 4**). This characterization holds for the interquartile range as well, except for the upper bound based on $C1\_q_{2m}$ scheme and the lower bound based on $C2\_q_{2m}$ scheme under the RCP 8.5 scenario over the last two epochs. There is no consistent, discernible impact of the RCP scenario on the multi-model median or range (interquartile or min/max) of the estimated trends/changes in the flood-producing event frequency across four scenarios. The only exception to that generalization is for $C1\_q_{2m}$, where the magnitude of the RCP8.5 lower bound is greater in magnitude than its RCP4.5 counterpart. Given all these considerations, there is no clear indication or likelihood of a "substantial" (i.e., ≥ 1 event) change in the occurrence of these events throughout the end of the century. These interpretations are based upon a pooled, averaged snapshot of the daily, atmospheric conditions across all the precipitation events

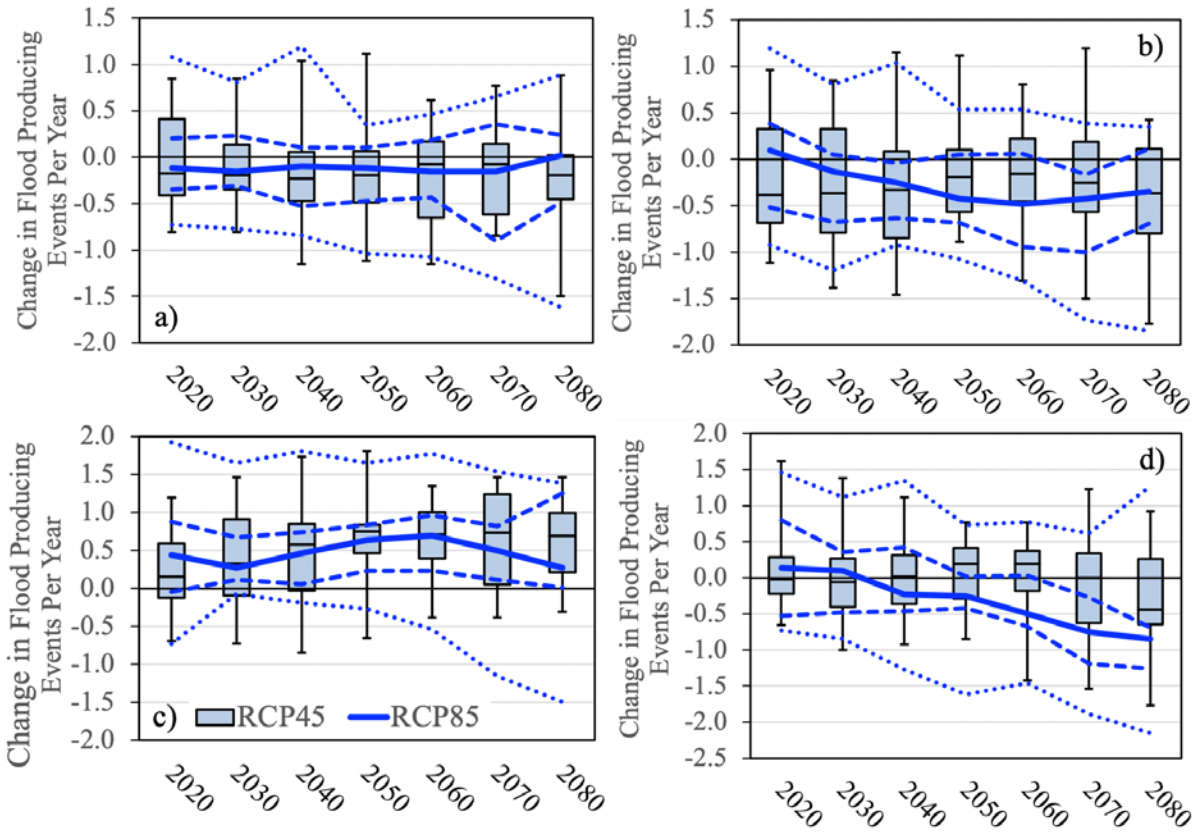

Figure 4. The estimated changes in flood producing event frequency based on the analogue schemes of a) C1_tpw; b) C2_tpw; c) C1_q_{2m}; and d) C2_q_{2m} for an ensemble of CMIP5 models under the RCP8.5 and RCP4.5 scenarios for JJA of Cambridge across the periods centered at year 2020, 2030, 2040, 2050, 2060, 2070, and 2080, respectively. The solid, dashed, and dotted blue lines represent median, Q1 and Q3, and minimum and maximum values, respectively.

that have been flagged (at ≥ 2"). We have not assessed what these patterns look like across all these events. It is likely that there are multiple patterns that can be "clustered". There may also be more rigor in the use of sub-diurnal atmospheric conditions - that during summertime conditions - are typically stronger controls to these precipitating events.

4. Summary remarks

This study has focused on assessing whether salient evidence exists that heavy-to-extreme precipitation events that have been observed across the greater Cambridge, MA area are expected to increase in frequency in the coming decades as a result of human-forced climate change. In doing so, we have employed an analogue-based procedure that empirically associates observed heavy-to-extreme summer precipitation events to large-scale atmospheric patterns. This analogue procedure is deliberately designed to leverage off the strength of general circulation models (GCMs) at reproducing large-scale atmosphere patterns – as opposed to the unresolvable spatial scales that summertime heavy-to-extreme precipitation events occur.

We find from the historical analysis that coherent, large-scale patterns of atmospheric conditions can be associated with heavy-to-extreme (i.e., ≥ 2" in three hours) summertime precipitation events. These patterns also indicate physically consistent conditions in the large-scale atmospheric conditions that support a warm, moist, and unstable environment that are required for intense precipitation events. We have used this information to calibrate similar information from the GCMs such that the occurrence of these patterns accurately reproduces the statistical frequency of the class of the summertime precipitation events of interest (i.e., ≥ 2" of rainfall in three hours). When we apply these associations to simulated future climates, we find that there is weak evidence of any considerable trend or change in the frequency of these events out to the end of the 21st century, and that the choice of whether these future climates consider strong or weak mitigation efforts has no salient effect on the ensemble-median change as well as the interquartile and minimum-maximum ranges.

Several considerations to this study warrant further investigation. First – the large-scale pattern associations are constructed from a pooled, mean of all the observed events. It is distinctly possible that each of these events did not occur from the "mean" conditions, but rather that they carried unique spatial features that were lost in the pooled means. Second, the atmospheric patterns used in the associations are based on daily mean outputs from the GCMs, and similar to the spatial aggregation, any sub-daily features of the atmospheric patterns that provide more rigorous predictive capacity has been lost. Thirdly, the approach identifies historical associations – therefore, any simulation of a future climate from a GCM that introduces an unprecedented (i.e., never-before observed) precipitation event with respect to its large-scale environment would not be captured by this procedure. However – the issue as to whether such a simulated event, from a coarse-resolution climate model, is realistic, plausible, and/or credible would need to be assessed. All of these considerations in a follow study could be addressed through augments and refinements to the statistical/machine-learning methods employed, more extensive model outputs provide by GCMs (through the CMIP6 exercise), as well as expanded observations.

Acknowledgments

This work was supported by the MIT Office of Sustainability (MITOS). The authors also wish to thank Brian Goldberg (MITOS) as well as Dr. Ken Strzepek for their intellectual support and guidance during the course of the study.

5. References

Bosilovich, M.G., R. Lucchesi and M. Suarez (2016). MERRA-2: file specification. GMAO Office Note No. 9 (Version 1.1), p 73. http://gmao. gsfc.nasa.gov/pubs/office_notes

Chen, C. and T. Knutson (2008). On the verification and compari- son of extreme rainfall indices from climate models. *J Clim* 21:1605–1621

Gao, X. and C.A. Schlosser (2019). Mid-Western US heavy summer-precipitation in regional and global climate models: the impact on model skill and consensus through an analogue lens. *Clim Dyn* 52, 1569–1582 doi:10.1007/s00382-018-4209-0

Gao, X., C.A. Schlosser, P. Xie, E. Monier and D. Entekhabi (2014). An analogue approach to identify heavy precipitation events: evaluation and application to CMIP5 climate models in the United States. *J Clim* 27:5941–5963

Gao, X., C.A. Schlosser, P.A. O'Gorman, E. Monier and D. Entekhabi (2017). Twenty-first-century changes in US regional heavy precipita- tion frequency based on resolved atmospheric patterns. *J Clim* 30:2501–2521

Gao, X., C.A. Schlosser and E.R. Morgan (2018). Potential impacts of climate warming and increased summer heat stress on the electric grid: a case study for a large power transformer (LPT) in the Northeast United States. *Climatic Change* 147, 107–118 doi:10.1007/s10584-017-2114-x

Molod, A., L. Takacs, M. Suarez and J. Bacmeister (2015). Development of the GEOS-5 atmospheric general circulation model: evolution from MERRA to MERRA2. *Geosci Model Dev* 8:1339–1356

Joint Program Report Series - Recent Articles

For limited quantities, Joint Program Reports are available free of charge. Contact the Joint Program Office to order.
Complete list: http://globalchange.mit.edu/publications

358. **Assessing the Changing Risk of Flood-producing Events in Cambridge.** *Gao & Schlosser, Mar 2022*
357. **The Changing Nature of Climate-Related Risks in Global Wind Power Resources.** *Schlosser et al., Feb 2022*
356. **Transition Scenarios for Analyzing Climate-Related Financial Risk.** *Chen et al., Jan 2022*
355. **Economic Analysis of the Hard-to-Abate Sectors in India.** *Paltsev et al., Sep 2021*
354. **Distributional Impacts of Low-Carbon Policies in USA and Spain: Does One Size Fit All?** *Garcia-Muros et al., Aug 2021*
353. **Predictability of U.S. Regional Extreme Precipitation Occurrence Based on Large-Scale Meteorological Patterns (LSMPs).** *Gao & Mathur, Jun 2021*
352. **Toward Resilient Energy Infrastructure: Understanding the Effects of Changes in the Climate Mean and Extreme Events in the Northeastern United States.** *Komurcu & Paltsev, Jun 2021*
351. **Meeting Potential New U.S. Climate Goals.** *Yuan et al., Apr 2021*
350. **Hydroclimatic Analysis of Climate Change Risks to Global Corporate Assets in Support of Deep-Dive Valuation.** *Strzepek et al., Apr 2021*
349. **A Consistent Framework for Uncertainty in Coupled Human-Earth System Models.** *Morris et al., Mar 2021*
348. **Changing the Global Energy System: Temperature Implications of the Different Storylines in the 2021 Shell Energy Transformation Scenarios.** *Paltsev et al., Feb 2021*
347. **Representing Socio-Economic Uncertainty in Human System Models.** *Morris et al., Feb 2021*
346. **Renewable energy transition in the Turkish power sector: A techno-economic analysis with a high-resolution power expansion model, TR-Power.** *Kat, Feb 2021*
345. **The economics of bioenergy with carbon capture and storage (BECCS) deployment in a 1.5°C or 2°C world.** *Fajardy et al., Nov 2020*
344. **Future energy: In search of a scenario reflecting current and future pressures and trends.** *Morris et al., Nov 2020*
343. **Challenges in Simulating Economic Effects of Climate Change on Global Agricultural Markets.** *Reilly et al., Aug 2020*
342. **The Changing Nature of Hydroclimatic Risks across South Africa.** *Schlosser et al., Aug 2020*
341. **Emulation of Community Land Model Version 5 (CLM5) to Quantify Sensitivity of Soil Moisture to Uncertain Parameters.** *Gao et al., Feb 2020*
340. **Can a growing world be fed when the climate is changing?** *Dietz and Lanz, Feb 2020*
339. **MIT Scenarios for Assessing Climate-Related Financial Risk.** *Landry et al., Dec 2019*
338. **Deep Decarbonization of the U.S. Electricity Sector: Is There a Role for Nuclear Power?** *Tapia-Ahumada et al., Sep 2019*
337. **Health Co-Benefits of Sub-National Renewable Energy Policy in the U.S.** *Dimanchev et al., Jun 2019*
336. **Did the shale gas boom reduce US CO_2 emissions?** *Chen et al., Apr 2019*
335. **Designing Successful Greenhouse Gas Emission Reduction Policies: A Primer for Policymakers – The Perfect or the Good?** *Phillips & Reilly, Feb 2019*
334. **Implications of Updating the Input-output Database of a Computable General Equilibrium Model on Emissions Mitigation Policy Analyses.** *Hong et al., Feb 2019*
333. **Statistical Emulators of Irrigated Crop Yields and Irrigation Water Requirements.** *Blanc, Aug 2018*
332. **Turkish Energy Sector Development and the Paris Agreement Goals: A CGE Model Assessment.** *Kat et al., Jul 2018*
331. **The economic and emissions benefits of engineered wood products in a low-carbon future.** *Winchester & Reilly, Jun 2018*
330. **Meeting the Goals of the Paris Agreement: Temperature Implications of the Shell Sky Scenario.** *Paltsev et al., Mar 2018*
329. **Next Steps in Tax Reform.** *Jacoby et al., Mar 2018*
328. **The Economic, Energy, and Emissions Impacts of Climate Policy in South Korea.** *Winchester & Reilly, Mar 2018*
327. **Evaluating India's climate targets: the implications of economy-wide and sector specific policies.** *Singh et al., Mar 2018*
326. **MIT Climate Resilience Planning: Flood Vulnerability Study.** *Strzepek et al., Mar 2018*
325. **Description and Evaluation of the MIT Earth System Model (MESM).** *Sokolov et al., Feb 2018*
324. **Finding Itself in the Post-Paris World: Russia in the New Global Energy Landscape.** *Makarov et al., Dec 2017*

MIT Joint Program on the Science and Policy of Global Change

Massachusetts Institute of Technology
77 Massachusetts Ave., E19-411
Cambridge MA 02139-4307 (USA)

T (617) 253-7492 **F** (617) 253-9845
globalchange@mit.edu
http://globalchange.mit.edu/